H.D. Hallen, "Ballistic electron emission microscopy: from electron transport studies to nanoscale materials science," a chapter for *The Technology of Proximal Probe Lithography*, edited by Christie Marrian, Vol. IS10 (SPIE, Bellingham, 1993).

Ballistic Electron Emission Microscopy: From Electron Transport Physics to Nanoscale Materials Science

H. D. HALLEN
Physics Division
AT&T Bell Laboratories
600 Mountain Avenue
Murray Hill, NJ 07974
USA

1. Introduction

The production of very small structure is now performed with a variety of approaches. The works described in this volume are a tribute to the growth of the field. But as the field advances it becomes increasingly important to optimize the creation of these structures, and to analyze the properties of the structures. The latter reason has not received as much attention as the former, but becomes critical when applications of the structures are considered. Small structures imply a high surface to volume ratio. In use, they are likely to be exposed to large current densities. Furthermore, the operation of small devices will probably depend strongly on the chemistry and physics of these structures, hence their characteristics must be measured and the relevant parameters identified for control.

It is not the aim of this chapter to solve all of the problems just mentioned. Rather we will discuss a new method with which one can do materials science at nanoscale resolution. Some examples will be given to illustrate the power of the method. The work focuses mainly on hot electron interactions with gold. It is shown that one can image structures on a buried interface and thus quantitatively measure hot electron stimulated atomic motion. The study of such properties at a buried interface is important from several considerations. The most obvious is that tip-sample or probe-sample interactions are absent. The high electric fields produced near an STM tip are also shielded. Thus the hot electron effects can be studied independently on the technologically relevant passivated interface. Vacancies produced in the hot electron scattering process build up in the film. Their presence can be detected. This opens the possibility of studying vacancy diffusion at very high resolution and at a known location -- be it well within a single grain or near a grain boundary. The question of how the structure will react to high current densities can

also be considered at a local scale. Our method is based on a recent extension of scanning tunneling microscope (STM) to observe subsurface properties known as ballistic electron emission microscopy (BEEM)[1. Although initially used to study Schottky barrier heights[1-5, the technique has also been demonstrated to be sensitive to interfacial transport[6,7, scattering in the film[6,8,9, diffraction at the interface[10, and interfacial structures[10-14. One can think of the method as a near field, few eV electron transmission microscope. The source of electrons is an STM tip, and the detector a Schottky barrier, as described in Section 2.3. Hot electrons injected by the STM tip can produce modifications of the gold film or its surfaces. Lower energy electrons are used to image the structures without further intervention. This paper will focus on modification of a gold film deposited on silicon. A carbon-based passivation layer lies between the film and substrate. The system will be described in more detail below.

The types of hot electron induced effects can be grouped into two categories: those that occur at a surface and those in the bulk of the film. Examples of each type are seen. By surface I refer to the outside of a grain: the top surface is the side of the grain scanned by the STM; the inner surface is opposite, i.e. at the interface of the gold and silicon; the grain boundaries are lateral surfaces which can be important during grain growth. At surfaces, the hot electrons induce the formation of adatom-vacancy pairs. The adatom is a gold atom which has moved out onto the surface. It may combine with other adatoms to form a terrace or diffuse to a sink such as a step edge, vacancy or grain boundary. The vacancy diffuses into the film. We have observed[10,11,13 terrace growth on the inner surface, grain growth on the lateral surfaces, and mound growth on the top surface of the films. The stability of the structure is found to depend strongly on the properties of the gold film.

The hot electrons can scatter from vacancies once they are in the bulk of the film. This can result in an enhanced, non-thermal motion of the vacancies. We have observed[10,11,13 the creation of large areas of defect-filled film. Such areas strongly scatter even lower energy electrons. The reaction of the system to the modification can be studied in real time. It will begin to react to the induced changes even while still under hot electron bombardment, and continue after the stress is removed. The reaction of the system can be a measure of the stability of the structures which were created, but also can reflect further development of the structures. One example of the latter occurs when several layers of terraces have been grown on the inner surface of the gold film, bringing the gold into contact with the silicon. As has been well documented[15, silicon will diffuse into a gold film evaporated into intimate contact with it, provided that the terrace is large enough. The resulting gold-silicon alloy scatters all electrons strongly. The resultant structure is very stable, much more so than the layers of terraces produced directly by the hot electron mechanism. A benefit of the BEEM technique is that the stability of bulk and subsurface interfacial structured can be observed in addition to the changes of the film topography. Through correlation between the observations one can gain an understanding of the mechanism by which mounds on metal surfaces are formed, and what the important parameters are in their decay. We believe that the BEEM technique will also be of aid in understanding other systems.

2. Experimental Technique

2.1 Detection of a Subsurface Terrace

In order to study the subsurface structures produced by the inelastic scattering of the hot electrons, it is necessary to be able to detect, with good sensitivity, buried structures which are only a single monolayer in height. The method we use is shown in Fig.□. The experimental situation will be described below, here we concentrate only on the contrast mechanism. A narrow beam of electrons is directed through the thin metal film. Those electrons which reach the interface must pass through a passivation layer which strongly scatters electrons. The thickness of the passivation layer will typically be a few monolayers and will scatter most of the electrons. The electrons which do not scatter are collected. To a good approximation, the passivation layer scatters electrons independent of the electron's energy[10. Thus a variation in the thickness of this passivation layer caused by the interposition of a terrace layer causes a large change in the magnitude of the transmitted current, so a measure of this current acts as a sensitive detector of single atom high terraces on the inner metal surface. Note that some amount of transmitted current is present in all parts of the trace. An image produced by measuring this current as the incident electron beam is rastered will provide a map of the interfacial or inner surface of the metal film, as is schematically indicated at the bottom of Fig.□.

To provide some experimental data to motivate this picture, consider Fig.□. Fig.□(a) shows a standard STM topograph of a sample described below consisting of a metal/passivation layer/semiconductor. Imaged at the same time is the transmitted current, measured from the semiconductor, shown in Fig.□(b). Each of the lighter regions in the figure corresponds to a single atom high terrace on the inner surface of the metal. In this case, the terraces were produced by stressing the interface with hot electrons from the STM tip, and the electron beam for imaging is also supplied (at lower electron energy) by the same tip. The transmitted current is approximately doubles when the tip is situated such that current will pass through a terrace region.

2.2 Sample Preparation

The general requirements of the sample have been outlined above: a thin metal layer, the system under investigation, lies on top of a few monolayer thick passivation layer with a semiconductor substrate. In this section, the material choices for each component will be discussed, in addition to other experimental considerations.

The metal is the system under study. We chose to study gold because of its technical importance and the fact that it is easy to study under ambient conditions -- most of this work was done on an STM operating in air. The thickness of the gold was taken to be 150□Å, which insured continuity while remaining on the order of one mean free path (~128□Å for this energy electrons[4) thick. The choice of semiconductor is determined by availability, quality, and the Schottky barrier height. Silicon was used in this study, giving a Schottky Barrier height of ~0.8□eV. As can be expected, the passivation layer has a dramatic effect on the interfacial modification processes. If the passivation layer consists of 1-2 monolayers of SiO2, no evidence of terrace growth is observed[11. We attribute this to the structure of the oxide -- it is not easily deformed to accommodate the terrace. Conversely, a monolayer of hydrogen[16 (or no passivation layer[11) is not

stable, and the entire sample degrades within a couple of days (or faster). We have grown samples in more elaborate structures than the metal/passivation layer/silicon described here to verify that the contrast in Fig. 2(b) is due to inner surface terraces[13, but will only describe the simpler case here. The work described in this chapter utilized carbon-based passivation layers. These were formed by allowing the sample to sit in a dirty vacuum for a few hours, and were analyzed with XPS[10, to find their composition and thickness (1-2 monolayers). Samples produced with an evaporated carbon passivation layers[13 (same thickness range) showed similar properties and magnitudes of transmitted current. This type of passivation layer was chosen since it was very reproducible[10, seemingly easy to deform to allow terrace formation, and the samples lasted a long time[10,14.

A flow chart illustrating the sample preparation process is shown in Fig. 3. As will be shown in Section 2.3, a small area device is necessary for experimental reasons. The small device is defined, the silicon rigorously cleaned[17, passivation layer added, and 150 Å thick gold film evaporated. The Schottky diode was then tested in a conventional probe station, where the current-voltage characteristic of the entire device was measured to obtain the average Schottky barrier height and the ideality factor (which was always close to one for these diodes). The sample was loaded into an STM/BEEM microscope described elsewhere[10, which was operated in air. Two qualitatively different types of gold films were used in this study. The first (type 1) was evaporated at 1 Å/sec in a high vacuum system. The grain size was typically one or a few hundred angstroms. Type 2 gold films were evaporated in UHV at a much slower rate 0.1 Å/sec to allow the film to anneal while growing. The grains were much larger (a few thousand angstroms), and presumable were cleaner and contained fewer point and line defects. It will be shown below that the stability of the structures depends strongly on the film characteristics, illustrating the relationship between bulk and surface in small structures and that this method can thus be a probe of bulk film characteristics.

2.3 BEEM

The BEEM process, including models which predict the shape of the BEEM current as a function of sample-tip bias, has been discussed previously[1,6,7. Therefore a short and rather heuristic treatment will be given here. The sample configuration for BEEM is the same as that used here, although the passivation layer is not required for all types of BEEM samples. A schematic drawing of the BEEM configuration is shown in Fig. 4(a). If one concentrates on just the tip and metal film, one finds that it is simply an STM operated in the constant tunnel current mode. The additional requirements for BEEM include the semiconductor below and another current preamplifier to detect the current that enters it. Thus, in BEEM, one can always acquire a constant tunnel current STM image of the surface of the film simultaneously with the BEEM current image, where the BEEM current is that current collected from the semiconductor. To determine the behavior of the BEEM current as a function of sample-tip voltage, consider Fig. 4(b). The tunnel bias controls the relative positions of the Fermi levels of the tip and metal film under investigation. The Schottky barrier is kept at zero bias, so one expects no BEEM current until the tip bias exceeds the Schottky barrier height (SBH). This is the case as indicated in the figure. The threshold current follows a $(eV\text{-}SBH)^2$ form at threshold then becomes linear in a simple effective mass model[1. Consideration of quantum mechanical reflection

at the interface[6,7 corrects the threshold form to (eV-SBH)$^{5/2}$. The images for this work were usually taken at 1.4□V and 1□nA, which is in the linear region of the BEEM spectra. Modifications were done at a higher bias where the simple model, which neglects resonant scattering in the metal, is questionable, as will be seen below.

From the above arguments, it is obvious that the BEEM technique is sensitive to the SBH of an interface. Other effects of the Schottky barrier are not as obvious, and vary for different types of samples. The Schottky interface provides a barrier to filter the electron distribution so that only those electrons within the proper (interface specific) transverse wave vector and energy range pass into the silicon. The BEEM current is that current which is collected in the silicon after having passed the Schottky barrier, so reflects the properties of the (sample dependent) filter. If one uses the BEEM technique on epitaxial sample for which the symmetry, size and orientation of the lattices on either side of the Schottky barrier is the same, symmetry arguments imply that the transverse wave vector of the electrons must be conserved as the electrons cross the interface. For systems with less symmetry, such as the Au/Si interface, one expects some relaxation of the momentum constraints, although some constraints remain[10. These transverse momentum constraints have an effect on both the shape of the BEEM spectra and the magnitude of the BEEM current[1,8. Thus, BEEM is an ideal tool to study the spatial variations of interface quality (or epitaxy) on a metal/semiconductor system. The shape of the BEEM spectra can be analyzed[6 to yield energy dependent transport properties of the interface. This chapter will not focus on the features of BEEM as a tool for Schottky barrier transport studies. Rather, it focuses on the effects of scattering within the metal film, which has effects on the scaling and shape of the BEEM spectra. This paragraph serves as a reminder of other effects to be considered during the measurement analysis.

The measurement criteria for BEEM require a quite tunnel current and a high gain current preamplifier[10. The tunnel current is controlled by the microscope design and the condition of the sample surface and tip. The sample has been described. We used electrochemically etched Pt tips. These performed well in air on the rough gold grains and was robust enough to perform reliably while operating at high bias for extended periods during sample modification. The noise in the measurement of the BEEM current is dominated by the Johnson current noise produced by the (zero bias) Schottky diode[10. To minimize this noise one must increase the resistance which can be done by lowering the temperature[4 or by decreasing the physical size of the diode[10. We chose the latter method which is the reason for the small metal contact discussed above.

2.4 Hot Electron Modification

One of the advantages of this technique is that the system can be modified by turning up the tunneling bias but imaged non-invasively when lower energy electrons are used. The damage induced by the hot electrons can be the creation of terraces on any surface of a grain, or the creation or stimulation of motion of defects within the film. These processes will be described below. Here the method used to stress the system with hot electrons will be outlined.

The STM is assumed to be tunneling to the sample with the sample to tip bias at the level used for imaging (typically ~1.4□V) which was chosen to be below any thresholds

for modifying the system. The tip is then scanned to the point where stressing is to be done. The sample to tip bias is swept to the stressing level at a rate slow enough that the feedback loop is able to maintain the constant current state. The voltage is held at this higher level for a specified amount of time - always with the feedback maintaining constant current. The tunnel bias is then reduced to the imaging value at the same rate as it was increased. An area scan measuring both the topography and a BEEM image is then taken, within a few minutes of the stressing. Subsequent images of the same region are often to taken to observe the stability of the structures. As will be discussed below, the created structures are usually stable but with important exceptions to be discussed below. The BEEM current is monitored during the entire time that the voltage is above the imaging value to provide real-time modification data which will be discussed below. The tunnel current is also monitored during the stressing and imaging to insure that it is being held constant by the feedback loop.

One can also modify a sample by sweeping a BEEM spectra to a very high bias. Some data of this sort will be shown below, but the interpretation of the real-time data is complicated by the usual variation of the BEEM current with voltage. One is also stressing with electrons of a range of energies.

An important insight into the nature of the process is found from calculating the number of electrons which are incident on the sample before it has time to relax. The tunnel currents used for modification were between 0.1 and 10□A, typically 1□A. For a 1□A tunnel current, the average time between electron arrivals is ~10^{-10}□sec for a region the size of the BEEM resolution. This time is much longer than electron relaxation times and phonon periods. Thus one would expect the electron system to have settled into an equilibrium or metastable state before the next electron arrives. The process results from the scattering of a single electron. As is expected for a single electron event, the relevant parameter is the dose of electrons, i.e. the product of the current and the time. This was verified experimentally[10.

3. Inner Surface Adatom Production

One of the most intriguing aspects of the present work is the fact that electrons injected into the gold when the bias is as low as ~1.8□V can stimulate the motion of gold atoms onto the inner surface. These adatoms then coagulate into terraces. The dynamics of the nucleation and initial growth periods can be observed in real-time by measuring the BEEM current while the stressing bias is applied. The growth of the terrace after it has become larger can directly yield a bound on the production rate of these adatoms. All these measurements can be made as a function of incident electron energy. As discussed in Section 2.2, we assume that the passivation layer has little effect on the process (as was discussed, this is true for this C-based but not all passivation materials). The passivation layer must be compressed or incorporated into the terrace to make room for the terrace as it grows.

The same adatom production process occurs at all surfaces of the film. Evidence is found in lateral grain growth and mound formation on the outer or free surface. The advantage of studying the buried surface is that the effects of the tip and electric fields are shielded.

Combining this with the comment at the end of Section 2.4: the phenomena is stimulated by a single hot electron at a time which scatters inelastically in a field free region.

3.1 Real-Time Observations of Terrace Nucleation

The modification which occurs due the stressing with hot electrons as described in section 2.4 can be followed in real time by monitoring the BEEM current. Experimental data are shown in Fig. 5(a). The results of this stressing was a net increase in the BEEM current in a region surrounding the tip location. Subsequent area scans showed terrace formation. Note that there are several distinct phases which occur while the voltage is held constant. These are labeled in a schematic drawing Fig. 5(b). Before describing the properties of each phase in detail, it is important to recall that the BEEM current is only sensitive to what is occurring in a region the size of the BEEM resolution (~10-20 Å in diameter) at the interface. We have seen that the modification process often creates structures much larger than this. The real time BEEM current plot will reflect only a fraction of this region, usually the center of the region unless the tip is nearly over a grain boundary. Following along Fig. 5(b), one finds that a latency period during which the BEEM current does not change follows the ramp to the stressing bias, then the current rises and saturates.

The latency period is best described by the picture in Fig. 6(a). Hot electrons are stimulating the production of adatoms at the inner surface of the gold. A vacancy must also be produced and is shown in the figure, its fate will be discussed in Section 4.1. When no terrace exists, the adatom will tend to diffuse away -- inhibiting the formation of a terrace. It is found that the latency time for a given dose depends on voltage in a roughly exponential manner as exp(-6.6±1.7V). This is shown in Fig. 7(a). One expects that the voltage dependence reflects the adatom production rate in some form, as will be verified below, but the latency time can be considered to reflect the time until a sufficiently large cluster of adatoms is built up to prevent a new one from freely diffusing away. When a new terrace is produced within 10-30 Å of a previous modification, a zero latency period is observed. In these cases, the nearby terrace presumably prevents the adatoms from freely diffusing.

When the BEEM current begins to rise, some adatoms must be localized at the inner surface underneath the tip. Fig. 6(b) depicts the situation. A small terrace has formed. The fact that the BEEM current is increasing implies that the terrace grows but is still smaller than the area to which the BEEM current is sensitive. The evaporation rate from such a small terrace is expected to be very high due to its thermodynamic instability[18. Thus, the initial growth rate of the terrace will be much slower than the growth rate when the terrace is larger. This is simply checked by comparing the time it takes for the real-time BEEM plot to saturate compared to the time it would take to grow a region the size of the BEEM resolution using the rates measured for larger terraces. One finds that the initial growth is ~10 times slower. A measure of the growth rate during nucleation is given by the time it takes for the BEEM current to reach half its saturated value, a quantity which behaves ~exp(-6.8±0.4V) up to ~2.5V stressing bias, as is seen in Fig. 7(b). The functional form of the current rise is approximately proportional to the square root of time.

After the real-time BEEM current plot saturates, the terrace is larger than the resolution of the BEEM technique. This provides a convenient way to measure the BEEM resolution. The stressing is stopped as soon as the BEEM current is found to saturate. A BEEM image shows the size of the structure. Subsequent images reveal if the terrace is evaporating or if it retains its size. This is the origin of the ~10-20 Å BEEM resolution quoted above.

3.2 Adatom Production

The growth of the terrace is measured in a BEEM image such as Fig. 2 as a function of electron dose and bias voltage. The initial increase of the area of the terrace is linear with the dose as is expected if the growth is limited by the adatom production rate. This can be seen in Fig. 3. The size of the terrace eventually saturates, probably due to annihilation of adatoms with vacancies from within the grain or loss of adatoms to nearby grain boundaries. The initial terrace growth rates can be converted into a lower limit on the adatom production rate. It is a limit since some adatoms are lost through annihilation with vacancies. The adatom production rate depends upon voltage as exp(5.9 V) at lower voltages, and begins to saturate ~2.5 V as is seen in Fig. 7(c). It is not surprising that the voltage dependence of the latency time, the rate of BEEM current rise and the adatom production rate all share the same voltage dependence. They all depend on the rate at which adatoms are produced.

One might wonder why diffusion does not play a role. The adatoms are created in the center of the terrace and must diffuse to the edge to increase the size of the terrace. The diffusion of gold atoms on gold is very fast for 'dirty' gold surfaces[18, i.e. outside of UHV. The presence of the passivation layer puts the inner surface in that class. Another, experimental, reason to believe that diffusion is fast on the inner surface is the length of the latency times (they would be very short if diffusion was slow) and the fact that it takes a long time for a second terrace to nucleate (more on this below). Note that the heuristic picture of adatoms being created at the center of the terrace, diffusing to the edge, and then falling off (or the equivalent vacancy diffusion from the edge to the center) may not be correct. Recent molecular dynamics calculations[19 suggest that a better picture for the decay of an upper gold terrace is that it falls straight down into the lower terrace, accompanied by a concerted motion of atoms in the lower terrace to make room for it. Thus the adatoms end up in the center of the terrace as opposed to the edges. If this picture is true, then very little diffusion is required, but the terrace atoms must make room for the adatom as it joins them. It is important to realize that the adatom must be an adatom (alone at the top of the terrace) at some point. Otherwise there would be no nucleation of the first and (as we will see below) further terrace layers in contradiction to experimental observations.

So far we have attributed the adatom-vacancy production to 'inelastic scattering of hot electrons.' A model has been proposed for this process[13. It is similar in nature to electron stimulated desorption (ESD), which has recently been reviewed[20. The difference from ESD is that the electron energies are much lower in the present investigation, and the ions are not ejected from the surface. The similarities are that an injected electron breaks a bond of an atom in the sample. This makes the atom unstable in the lattice -- it

undergoes a Franck-Condon transition. A picture is given in Fig. 9. The atom was originally sitting in a potential well formed by the bonding to its neighbors. When the bond is broken, it shifts to the upper potential energy curve which is shown for a surface atom. If the bond remains broken for a long enough period of time for the atom to be accelerated by the potential energy gradient and move out onto the surface, an adatom-vacancy pair will have been created. Typically a bond will not remain broken for such a long time unless it has been stabilized by a lattice distortion. Instead, the hole (broken bond) will jump from one atomic site to another through the lattice until either it is localized or decays. Atoms near surfaces or defects in the bulk (e.g. vacancies) do not have as high a coordination number so generally have softer bonds than other atoms. These bonds can therefore deform more easily to localize the hole than others. Thus a hole created in the bulk of the film can move to a defect or surface and get localized. If it is too far away, however, it is likely to decay on the way. We hope to be able to measure such decay lengths and localization probabilities in the future using this BEEM technique with an appropriate range of samples. Some discussion of hole localization is given in Ref. [20]. One remark is in order before leaving the subject of localization. In a metal, one normally thinks of electrons as being very delocalized, so the idea of a localized hole is counter-intuitive. What we are proposing is a hole in the d-band of the gold. This band has a narrow width (it is more like a core electron) so the electrons are in fact more localized than the conduction electrons.

A model to predict the voltage dependence of the adatom production rate was given in Ref. [13]. The model used an approximate calculation of the hole formation rate at finite temperatures for a system with a gaussian broadened threshold energy. A broadened threshold for hole creation is not unrealistic: the bonds involved are near defects so are strained and in a variety of environments. The model predicts a nearly exponential voltage dependence below threshold, with the exponential factor depending on temperature and the width of the threshold distribution. A good fit to the latency time, half-time for BEEM current rise and the areal growth rate of the terraces, all of which depend on the adatom production rate, is found for a broadened threshold centered at 2.5 eV with a full width of 0.4 eV. This fit is shown as a solid line through the data in Fig. 7. Theoretical band structure calculations for gold[21 are consistent with a ~2.5 eV energy between the d-bands and the Fermi level.

There is another measurement which can be done to give an independent estimate of the threshold energy distribution. This is to sweep the sample-tip bias to very high values and look for a decrease in the BEEM current which ought to occur when the incident electrons resonantly scatter to produce electron-hole pairs. If a significant fraction of the secondary electrons do not cross the Schottky barrier to become part of the BEEM current (Section 2.3 gives good evidence why they shouldn't in this energy regime), then an obvious dip should be seen. This type of measurement is not easy to make since the resonant scattering can easily change the sample so that the BEEM current drops or goes away (more on this in Section 4). Thus the spectra are not always repeatable and can have a variety of shapes[10. Nevertheless, one particular type of BEEM spectra is seen much more frequently than the others. It has been seen on several samples with several tips so can be considered the typical case. It is shown in Fig. 10. The BEEM current does indeed decrease in the neighborhood of 2.5 V in agreement with the above threshold value. There is also another decrease in the BEEM current at ~3.8 V. This is close to the value of

another vertical transition between two high density of states points in the band structure[21, giving further evidence that these BEEM spectra features arise from electron-hole pair formation (electron-electron scattering) in the gold.

3.3 Control and Reproducibility

At the bottom and right hand sides of Fig. 11 are some terraces which appear as lines. These are literally the first attempts at making any structures besides dots with the technique. First the line near the bottom was made by positioning the tip at the left end, raising the tip bias to 2.3 V @ 1 nA tunnel current, and moving 700 Å to the right at 230 Å/sec and back to the starting position at the same rate. When no increase in BEEM current under the tip was observed, the tip was swept again to the right at 47 Å/sec, leaving the line in the figure. The lines at the right of Fig. 11 were formed by moving to the right hand end of the upper line, where the tip bias was increased to 2.3 V @ 1 nA tunnel current. The line segments were then swept in order -- the last one is vertical in the image right at the edge of the figure. The horizontal lines are 350 Å long and the vertical lines 400 Å long, all swept at ~30 Å/sec. This demonstrates the extreme control and reproducibility of the phenomenon.

In principal, arbitrarily shaped and sized structures can be created. The limitation is thermodynamic stability of the structures, i.e. they must be large enough that surface energy does not cause them to evaporate, and diffusion rates of both the terrace atoms on the surface and vacancies within the film. Stability issues will be discussed in Section 5.

3.4 A Second Layer

Since a single atomic layer high terrace can be grown so easily, it is natural to expect that a several atomic layer high terrace could be grown. Since the adatom sink into the first terrace is much faster than adatom loss to grain boundaries, one would expect that a significantly higher adatom production rate would be required to nucleate a second layer. This is true experimentally. One might also expect that the BEEM current under the second layer would be much higher than even that where a single atomic layer high terrace exists, i.e. one would expect a tiered structure from where there are no, one, and two atomic layer high terraces. This is not found experimentally. Rather, a region of very small or no BEEM current is found where the two atomic layer high terrace exists. This can be understood in terms of gold-silicon interdiffusion[15, which occurs when enough gold comes into intimate contact with silicon. Images of such structures are seen in Fig. 11. The behavior is due to diffusion of silicon into the film, so will be discussed in Section 4.2.

4. Bulk Effects

Scattering in the bulk of the film reduces the number of electrons which reach the interface to attempt to cross it, so therefore reduces the BEEM current (although this seemingly obvious statement is true in this case, momentum conservation at the interface and the incident electron distribution can conspire to reverse the result in some systems[8). A schematic drawing of the situation is shown in Fig. 12. Two types of

bulk scattering processes are shown. One results from scattering throughout the film, and one from scattering in a near-interfacial layer. Both types are observed in the Au/passivation layer/Si system. The methods of identifying the scattering source and distinguishing between the two will be discussed in Section 4.3.

4.1 Vacancies

A vacancy production always accompanies the production of an adatom if the terrace made from the adatoms is to grow. This vacancy diffuses into the 'bulk' of the film. A hot electron can scatter from a vacancy similarly to the way it scatters at the inner surface, so one would expect that whenever a vacancy gets into the (resolution-sized) region in the path of the incident electrons, it would decrease the BEEM current. One would expect to observe this phenomena during and after the modification process. Bursts of such decreases in the BEEM current are seen during all parts of the real-time BEEM plot. Examples are shown in Fig. 13. Some are found near the end of the latency period in Fig. 13(a), and some in the saturated region of Fig. 13(b). Note that the vacancy scattering stops after a short period. This means that the vacancy has become trapped or has moved out of the path of the incident electrons.

It is not surprising that the effects of vacancies are observed during the modification. The electrons can scatter nearly resonantly from the vacancies so even a small vacancy density should be observable. It is also possible to see the effects of a high density of vacancies with the (~1.4 V bias) electrons used for imaging. This requires a high density of vacancies. The mechanism is strong scattering which decreases the number of electrons which can cross the Schottky interface. Such a high density of defects is unstable, and will anneal. Experimentally, the annealing time (observed by changes in the BEEM image) is of order minutes, and is accompanied by changes in the topography (observed in the constant current STM image). This has been observed on both type 1 and type 2 gold films.

An example of such a high density of vacancies in a type 2 film is seen in Fig. 14. The STM tip was centered over the region shown in the image of Fig. 14(a-b) while the bias voltage was held at 3.5 V for 3 sec while a constant current of 1 nA was maintained. Comparing the topographic images Fig. 14(a,c), one finds that the grain has been puffed up. In reality it has been filled with vacancies. The corresponding BEEM images Fig. 14(b,d) show how the lower energy (1.4 V bias) electrons are scattered by the vacancy structure. In subsequent images, the region of decreased BEEM current is seen to decrease until it is eventually gone. The lateral size (diameter) of this region decreases linearly in time[13 from the edges inward at a rate of ~32 Å/min. The grain in the STM image which was puffed up by the hot electron stressing decreases in size until it no longer appears as a lump by the time the BEEM image has healed. This observation underlines the reversibility of the vacancy motion process.

In type 1 films, the situation is less dramatic. Usually a second layer terrace has grown and intermixing occurred before such a high density of defects has been created (Section 5). Some additional decrease in the BEEM current is seen due to vacancies, which heals at about the same rate as the type 2 structures. The entire grain does not

expand. Instead, a mound forms over part of the grain, or several nearby grains. This mound changes slightly during the annealing process, but does not disappear completely.

4.2 Highly Scattering Interfacial Layers

The formation of an interfacial layer which scattered electrons strongly was discussed in Section 3.4. The second layer terrace brings the gold into intimate contact with the silicon over an area large enough that the silicon bonding is disrupted and diffuses into the gold. The resulting high density of impurities in the gold greatly increases the elastic scattering rate resulting in a decreased BEEM current. A schematic drawing is shown in Fig. 2(b). Examples of BEEM images are shown in Fig. 1.

Interfacial reactivity such as that observed here with very high lateral resolution is common. BEEM is a powerful technique to probe such systems, as the transmission of electrons through an interface will usually be strongly effected by any interfacial reaction. In contrast to the unstable vacancy structures, this type of modification is irreversible at room temperatrue by the second law of thermodynamics.

Information about the thickness and growth of the interfacial layer may be obtainable from the real-time BEEM current as such a modification is produced. Such a real-time BEEM current plot is given in Fig. 5(a). The BEEM current decreases to a saturation level. This decrease is exponential in time as is expected if a layer of material with a short mean free path was growing in thickness. In this case, the material is silicon intermixed with gold. The method is equally suited to measure other materials.

4.3 Identifying the Type of Modification

Two distinct mechanisms which produced local degraded regions in the BEEM image have just been described. We saw that one type (high defect density within the film) is reversible whereas the other is not. This provides one method of determining the type of modification. The highly scattering interfacial layer is produced by terrace layer growth so is found in connection with an enhanced region. This also serves as an indication of which type of modification is present. But one would like to have other methods to distinguish between the two. It is probable that both types of modification are present in some cases. If one observes a stressed region for several minutes after stressing, one often finds a slight change in the BEEM image accompanied by a change in topography[10. This is almost certainly due to the healing of vacancy structures within the gold film as described above in Section 4.1. The remaining structure (none in the case of Fig. 4) could be due to intermixing at the interface or the stabilization of a vacancy structure by some other defect (such as a line defect).

There is another way to distinguish the two processes. The BEEM current can be monitored during the production of the degradation structure. Well-defined signatures allow one to predict whether the mechanism will be intermixing at the interface or vacancy structures within the gold. In general, the interfacial mixing process has a less dramatic effect on the BEEM current than does dense vacancy formation. This is not surprising since the strongly intermixed layer remains near the interface (or there would be no reason for there not to be enough lateral growth to cover and destroy the enhanced

region where only one terrace layer exists) whereas the defects can scatter the injected electrons for the entire thickness of the film. This can be seen in Fig. 15. Real-time BEEM current plots during stressing are shown in Fig. 15(a-b). A much faster and sharper drop is observed in Fig. 15(b), which left a mound and presumably many defects within the film, compared to Fig. 15(a), which left an intermixed interfacial layer type modification. BEEM I-V spectra are shown in Fig. 15(c-d). The data are shown for the entire time the sample-tip voltage was different from the imaging bias of 1.4 V. Different symbols are used to differentiate the different directions of voltage sweep. Comparison of the starting and finishing values of the BEEM current in Fig. 15(c-d), both taken at the imaging bias, one sees that the BEEM current has decreased in the region under the STM tip. The result of the stress shown in Fig. 15(c) was an intermixed region. A highly defected film as evidenced by the STM and BEEM images was obtained following the sweep in Fig. 15(d). Note the sharp drop in the BEEM current as the vacancy structure has grown before the bias is decreased. A subsequent BEEM I-V extending to a lower maximum bias exhibits a different spectral shape near the Schottky barrier height threshold.

Finally, we comment that in the case of a type 1 gold metal layer under study, it appears that a second terrace layer (and hence a highly intermixed interfacial region) can be nucleated at a lower bias than is needed to create a substantial defect structure within the film. Note the very high bias (3.5 V) required to fill the grain in Fig. 14 with vacancies compared to the value (~2.5 V) at which the second layer formation is first observed in the type 1 samples. Type 1 samples stressed at very high biases also show a large amount of mound formation and some subsequent healing. These observations illustrate that one has some degree of control of which type of structure is produced by managing the sample and stressing characteristics.

5. Stability and Materials Dependence

The effects of the interface chemistry and structure on both the stability of the BEEM interface and the modification phenomena have been discussed in Section 2.2 and elsewhere[10,11. Thus the discussion here will be limited to the effects of the gold film. The stability of the structures created within the film or on any of the surfaces is strongly tied to the nature of the film itself. This is why the title of this section couples the two together. Two types of gold films were used in this study as discussed in Section 2.2.

The inner surface structures are quite stable on a type 1 film. The terraces of Fig. 2 and the lines and other modifications in Fig. 11 stay close to their original form for at least hours (as long as we cared to observe them). In contrast, inner surface terraces on type 2 samples are not stable but decay very quickly[13. The rate of decrease of the diameter can be as fast as 1 Å/sec. Afterwards, the interface is much as it was before production. We interpret the difference in stability to the difference in vacancy diffusion rates. Vacancies can diffuse much more easily in the clean type 2 films. Once a vacancy reaches the inner surface, it can recombine with a terrace atom to decrease the size of the terrace.

Vacancy structures within the films anneal at least somewhat in both types of samples. The time constant of change seems to be about the same, a few minutes, in both cases.

An example of this behavior in a type 2 film was shown in Fig. 4. In the type 2 films, where interfacial intermixing is not observed, the BEEM image returns to its initial (before stressing) form. Thus one can rule out the existence of a stabilization of remaining defects. Such a stabilized structure cannot be ruled out in the type 1 films, as a degradation from an interfacial intermixed layer remains.

Mound formation on the top surface of the film is also seen to differ. Whole grains are effected uniformly in the type 2 films as seen in Fig. 4. Type 1 films show mounding within a grain, Fig. 1. The mounds on a type 1 sample do not anneal away completely (just slightly) on the minutes time scale, but instead last at least a few hours. The differences in mound formation between the two types of gold probably reflect differences in the quality of the film. They may partially be due to length scales, however. It may be possible to create a mound within a grain of a type 2 film if the grains were large enough, e.g. if the sample was epitaxial.

The question of why no interfacial intermixing modification was observed in type 2 samples deserves further comment. If a second layer terrace grows on the inner surface bringing the gold into contact with the silicon, we expect intermixing. Thus we can reword the question to : Why doesn't a second layer nucleate on the inner surface of type 2 films? The answer is related to the stability of the terraces as discussed above. Terraces are rapidly being annihilated on the type 2 films, even as the terraces grow. Thus it ought to take a much higher adatom production rate to compensate for the loss to both grow and keep the lower terrace large, so it does not sink the adatoms from the layers above, and to provide a high enough density to nucleate at the second level. The problem is that vacancy structures form at these higher biases. The vacancies scatter hot electrons even before they reach the inner surface, so effectively decrease the rate of adatom production. Thus one is not able to maintain the rate of adatom production to nucleate a second layer in the type 2 samples. The terrace annihilation rate is very small for the type 1 samples, so it does not need to be compensated for and terraces can be nucleated.

6. Electrons or Holes

A technique related to BEEM, but using the reverse tunnel bias from that which one would normally expect to get a BEEM current, has recently been demonstrated[9. In our samples, this corresponds to injecting holes into the gold from the tip. We use the term Auger BEEM to describe the measurement since the BEEM current arises from secondaries (Auger electrons) which are formed as holes scatter and are filled by electrons from near the Fermi level. Thus one obtains a current with the same sign as that observed with normal-BEEM, but the tip bias is reversed. The detailed threshold shape has been predicted[9, and images are collected in much the same way as in normal-BEEM.

It is interesting to compare the modification behavior of the sample under the injection of hot holes to that observed under hot electron injection. Real-time BEEM plots during Auger BEEM stressing do not look like those in Figs. 3,13. The BEEM current rise is lacking. Instead, the BEEM current drops after a latency period[11. As above, the latency time and rate of BEEM current decrease depend strongly on voltage. Subsequent Auger-BEEM images show a degraded region, but no change is observed in before and after

normal-BEEM images[10. This suggests that the imaging mechanism differs between normal and Auger BEEM. The contrast in normal BEEM images of Au/Passivation layer/Si samples is dominated by the interface, although very high defect densities can effect the images. In contrast, we believe that the formation of the Auger electrons dominates the contrast in the Auger-BEEM images. The absence of terrace growth (as imaged by normal BEEM) by Auger-BEEM or hole-injection suggests that the holes scatter much more closely to the top surface than the inner surface. The result that electrons scatter more strongly is reasonable considering the ESD model where the electrons create holes that stimulate the atomic motion. It also suggests a source of the contrast in the Auger-BEEM images. The atomic motion process would compete with or substantially alter the formation of Auger electrons. Thus even a small density of defects could strongly decrease the Auger-BEEM signal while not greatly effecting the imaging energy electrons used to form the normal-BEEM image. This accounts for the paradox of why normal-BEEM does not detect a hole injection modification detected by Auger-BEEM, and suggests the physical nature of the modification produced by hole injection.

7. Mound Formation

The creation of mounds on gold surfaces with STMs has received much attention in the past few years, a few examples are given in Ref. 22-23. In particular, by varying the parameters to make a 'recipe', extremely reproducible results are obtained[23. It is interesting to compare the other mound formation work to that presented here. Mound formation has been observed in this work, as has motion of gold at the inner surface of the samples. The motion of gold at the inner surface is the result of inelastic scattering of the hot injected electrons. There are no tip-sample or tip electric field effects at the inner surface. We suggest that the motion of gold to produce the mounds is caused by the same mechanism, as is strongly suggested by this work. This represents a new model for mound formation. A previous paper[23 suggested that the cause was field induced evaporation of gold from the tip to the sample. None of the previous studies controlled the tunnel current as the bias was raised. The tunnel currents during mound formation were very large. Voltage was controlled, however, and mound formation was observed above a threshold near 3.2-3.5 V. The field evaporation model was not able to explain such a low threshold voltage. The threshold value is roughly what one would expect for massive gold movement within the model presented here (Fig. ,14), which suggests that the same mechanism may explain all the mound formation work. We have observed a bias sign dependence on the threshold at which mound formation is clearly evident. A bias of ~2.5 V positive sample-tip bias or ~2.1 V for negative sample-tip bias. This is consistent with the idea of holes scattering closer to the top surface than electrons, as discussed in the last section. The nature of the gold must also be considered. We observed a strong dependence of the modification and mound formation properties as a function of gold quality(Section). We do not know the cleanliness of the gold in the other works. Note that the fact that mound formation can be observed on very thick or bulk gold samples does not preclude the inelastic scattering and vacancy motion model described here. We expect adatom-vacancy pairs to be generated at all gold surfaces, including the top one which is present in all the studies.

8. Summary

The BEEM technique has been shown to be a powerful technique for studying hot electron scattering in a thin metal layer in addition to providing high lateral resolution measurements of diffusion of defects within the film and interdiffusion of species at a buried solid-solid interface. We have shown that hot electrons injected by an STM tip scatter and modify a gold film throughout its volume and at all its surfaces. The BEEM measurement technique is found to be a powerful method for probing such buried structures. With an appropriate choice of passivation layer between a gold film and silicon substrate, small single atom high terraces on the inner surface of the gold can be studied. This is important as it allows observation of hot electron effects at high spatial resolution without the effects of a high electric field from an STM tip or other tip-surface interactions. The nucleation and initial growth of buried-surface terrace structures is observed in real-time. One can measure the effects of the thermodynamic instability of the initially very small terraces by comparing the initial growth rate to the growth rate of larger terraces. The growth rate is related to the rate of adatom production, which can be determined quantitatively as a function of voltage from such measurements. Vacancy formation accompanies adatom formation. The structures formed by the vacancies can effect the BEEM images, which then allows a glimpse into their evolution. The BEEM image is correlated with an STM image to relate vacancy structure changes and topographic changes. The mechanisms of mound formation and stability can be addressed. The stability of the created structures is shown to be related to the physical properties of the gold film.

9. Future Outlook

The work discussed in this chapter shows many possible applications of the BEEM technique for studying transport and materials science at nanoscale resolution. The healing of defect structures made of a high density of defects and the annihilation of terraces by vacancy diffusion suggest a new way to study vacancy diffusion within a single grain. One can see where the grain boundaries are in the STM image, so their effect can be studied as well but independently. This will require careful analysis of the BEEM current image change as a function of time after modification. Diffusion of gold on the inner surface could be investigated, as can grain growth.

Electron transport issues can be addressed. BEEM can measure the Schottky barrier heights[1. Quantum effects in interface transport can be studied[6. By choosing an appropriate system, e.g. a lattice matched interface and a particular substrate orientation, transverse momentum constraints can become crucial for electron transport. This can emphasize elastic scattering in the film[8, or can be used to probe interface quality -- in regions where the interface is rough, transport constraints will change so one can expect a change in the BEEM current magnitude and spectral shape. Interfacial reactions may also be evident as a change in BEEM current as discussed in this chapter. Questions such as how hot electrons scatter and what is the effect on the film microstructure can be answered. One can even hope to gain some better understanding of the electromigration process using BEEM as a tool.

For the purposes of this book, we should comment that the structures produced by proximal probe techniques are very small but need to be characterized. BEEM related techniques may be able to do that, and further may be able to pinpoint mechanisms for growth, such as the mound formation discussed herein. The high surface to volume ratio of the structures we are producing may change the materials characteristics from bulk-like to surface dominated. This is a new regime for materials study, and tools need to be developed to provide physical insight and data for theoretical testing. The small structures will be asked to carry high current densities. We need to characterize the effects of such electron transport to identify which processing methods yield materials suitable for use, and what are the expected lifetimes of the structures. Note that the BEEM technique described here does not require very specialized samples. Metal on top of silicon occurs frequently in devices; an area of silicon could be doped and such devices fabricated on-chip if need be to address film quality issues.

10. Acknowledgments

The experimental aspectsa of this study were completed while the author was at Cornell University, in collaboration with Tony Huang, Andres Fernandez and R. A. Buhrman. We wish to acknowledge constructive discussions with David Peale, Wilson Ho, John Silcox, and Dan Ralph. We thank Bill Kaiser, Carl Kukkonen and the Jet Propulsion Lab for helping us to get started in STM. During part of the time this work was done, HDH was supported by an IBM Graduate Fellowship. Research support was provided by the Office of Naval Research. Additional support was provided by the National Science Foundation through use of the National Nanofabrication Facility and the facilities and equipment of the Cornell Materials Science Center.

11. References

[1]. W. J. Kaiser and L. D. Bell, 'Direct investigation of subsurface interface electronic structure by ballistic-electron-emission microscopy,' Phys. Rev. Lett. **60**, 1406-1409 (1988); and L. D. Bell and W. J. Kaiser, 'Observation of interface band structure by ballistic-electron-emission microscopy,' Phys. Rev. Lett. **61**, 2368-2371 (1988).

[2]. M. H. Hecht, L. D. Bell, W. J. Kaiser, and F. J. Grunthaner, 'Ballistic-electron-emission microscopy investigation of Schottky barrier interface formation,' Appl. Phys. Lett. **55**, 780-2 (1989); M. H. Hecht, L. D. Bell, W. J. Kaiser, and L. C. Davis, 'Ballistic hole spectroscopy of interfaces,' Phys. Rev. **B42**, 7663 (1990); and . T. H. Shen et al., 'Ballistic electron emission microscopy, current transport, and p-type δ doping control of n-isotype InAs-GaAs heterojunctions,' J. Vac. Sci. Technol. **B9**, 2219-24 (1991).

[3]. Y. Hasegawa et al., 'Ballistic electron emission in silicide-silicon interfaces,' J. Vac. Sci. Technol. **B9**, 578-80 (1991); A. Fernandez et al., 'Ballistic electron emission microscopy studies of the $NiSi_2$/Si(111) interface,' J. Vac. Sci. Technol. **B9**, 590-93 (1991); and Philipp Niedermann et al., 'Ballistic electron emission microscopy study of PtSi-n-Si(100) Schottky diodes,' J. Vac. Sci. Technol. **B10**, 580-5 (1992).

[4]. L. D. Bell, W. J. Kaiser, M. H. Hecht, and L. C. Davis, 'New electron and hole

spectroscopies based on ballistic electron emission microscopy,' J. Vac. Sci. Technol. **B9**, 594-600 (1991).
[5]. A. E. Fowell et al. Semicond. Sci. Technol. **5**, 348 (1990); A. E. Fowell et al., 'Ballistic electron emission microscopy studies of Au-CdTe and Au-GaAs interfaces and band structure,' J. Vac. Sci. Technol. **B9**, 581-84 (1991); and M. Prietsch, A. Samsavar and R. Ludeke, 'Structural and electronic properties of the Bi/GaP(110) interface,' Phys. Rev. **B43**, 11850-6 (1991).
[6]. H. D. Hallen, et al., 'Scattering and spectral shape in ballistic electron emission microscopy of $NiSi_2$-Si(111) and Au-Si samples,' Phys. Rev. **B46**, 7256-59 (1992).
[7]. M. Prietsch and R. Ludeke, 'Ballistic-electron-emission microscopy and spectroscopy of GaP(110)-metal interfaces,' Phys. Rev. Lett. **66**, 2511-14 (1991); L. J. Schowalter and E. Y. Lee, 'Role of elastic scattering in ballistic-electron-emission microscopy of Au/Si(001) and Au/Si(111) interfaces,' Phys. Rev. **B43**, 9308-11 (1991); M.D. Stiles and D. R. Hamann, 'Kinematic theory of ballistic electron emission spectroscopy of silicon-silicide interfaces,' J. Vac. Sci. Technol. **B9**, 2394-8 (1991); and E. Y. Lee and L. J. Schowalter, 'Electron-hole pair creation and metal/semiconductor interface scattering observed by ballistic-electron-emission microscopy,' Phys. Rev. **B45**, 6325-28 (1992).
[8]. A. Fernandez et al., 'Elastic scattering in ballistic electron emission microscopy studies of the epitaxial $NiSi_2$/Si(111) interface,' Phys. Rev. **B44**, 3428-31 (1991).
[9]. L. D. Bell, M. H. Hecht, W. J. Kaiser, and L. C. Davis, 'Direct spectroscopy of electron and hole scattering,' Phys. Rev. Lett. **64**, 2679-82 (1990).
[10]. H. D. Hallen, Ph.D. thesis, 'Ballistic electron emission microscopy studies of gold-silicon interfaces,' Cornell University, January 1991.
[11]. H. D. Hallen, et al., 'Gold-silicon interface modification studies,' *Proceedings of the Fifth International Conference on Scanning Tunneling Microscopy/Spectroscopy*, (Baltimore, July 23-27, 1990) in J. Vac. Sci. Technol. **B9**, 585-589.(1991); and 'Ballistic electron emission microscopy of metal-semiconductor interfaces,' *Proceedings of the Ballistic Electron Emission Microscopy Workshop 1990* , Jet Propulsion Laboratory, California Institute of Technology, Pasadena, CA, March 9, 1990.
[12]. M. H. Hecht et al., in *Proceedings of the Ballistic Electron Emission Microscopy Workshop 1992* , Death Valley, CA, January 27, 1992.
[13]. H. D. Hallen and R. A. Buhrman, 'Hot electron induced atomic motion and structural change at the passivated gold-silicon interface,' (submitted).
[14]. H. D. Hallen and R. A. Buhrman, 'BEEM: A probe of nanoscale modifications,' to appear in the *NATO Advanced Studies Institutes* series, edited by Ph. Avouris (Kluwer, Dordrecht).
[15]. For example L. J. Brillson, A. D. Katnani, M. Kelly, and G. Margaritondo, J. Vac. Sci. Technol. A **2**, 551 (1984).
[16]. W. J. Kaiser and L. J. Schowalter, private communications.
[17]. A. Ishizaka and Y. Shiraki, J. Electrochem. Soc. **133**, 666 (1986).
[18]. D. Peale and B. H. Cooper, (private communication); and D. Peale, Ph.D. thesis, 'Diffusion and mass flow dynamics on the gold (111) surface observed by scanning tunneling microscopy,' Cornell University, January 1992.
[19]. U. Landman, 'Atomic-scale dynamics and stability of interfacial systems and nanostructures,' to appear in the *NATO Advanced Studies Institutes* series, edited by Ph. Avouris (Kluwer, Dordrecht).

[20]. R. D. Ramsier and J. T. Yates, Jr. 'Electron-stimulated desorption: principals and applications,' Surface Science Reports **12**, 243-378 (1991).
[21]. N. Egede Christensen and B. O. Seraphin, 'Relativistic band calculation and optical properties of gold,' Phys. Rev. **B4**, 3321-44 (1971).
[22]. David W. Abraham, et al., 'Surface modification with the scanning tunneling microscope,' IBM J. Res. Develop. **30**, 492 (1986); Y. Z. Li et al. 'Writing nanometer-scale symbols in gold using the scanning tunneling microscope,' Appl. Phys. Lett. **54**, 1424 (1989).
[23]. H. J. Mamin, P. H. Guethner, and D. Rugar, 'Atomic emission from a gold scanning-tunneling-microscope tip,' Phys. Rev. Lett. **65**, 2148-21 (1990).

Figure 1. A schematic drawing which illustrates how an inner surface terrace can increase the BEEM current due to a high scattering rate in the passivation layer material which it displaces. The BEEM electrons pass through a thinner layer of passivation material where a terrace exists. The electrons which are scattered back, in addition to many which cross the passivation layer but are not able to surmount the Schottky barrier, are eventually collected to maintain the tunnel current.

Figure 2. 1. Gray scale 1.4□V constant 1□nA current STM (left) and corresponding BEEM (right) images illustrate enhancement type modifications of a type 1 sample. The images are 800□Å square. (a) shows the STM topograph which did not visibly change as a result of the modifications. (b) is the BEEM image where all the whitish areas were individually created by stressing with the STM current. The BEEM image before any stressing was uniformly gray. Clockwise from the two largest (just touching, in the lower left) the modifications were created with a 2.5□V for 3.8□sec, an voltage sweep 0.4->2.88□V in 5.7□sec, 2.1□V for 6.7□sec, 2.0□V for 6.5□sec, 2.25□V for 3.3□sec, and the at the bottom center 2.25□V for 7.0□sec.

Figure 3. A flow chart illustrates the various sample preparation steps. At the right is a schematic drawing of the sample at each stage.

Figure 4. The BEEM measurement technique is illustrated by (a) a schematic drawing of the sample and amplifier configurations. The STM tunnels into a thin metal film. The BEEM current is collected from the semiconductor substrate. Typical parameter values are shown. (b) A band structure drawing illustrates the energetic considerations of BEEM. It can be used to estimate the structure of a BEEM current vs. sample-tip voltage spectra as is shown in (c).

Figure 5. The BEEM current is monitored in real-time during modifications of the sample. The sample-tip bias was increased from the imaging value of 1.4□V linearly to the stressing value, at which it was held constant for a period of time, then decreased linearly back to the imaging value. The dotted lines indicate the times at which the bias reached and left the highest stressing value. (a) Experimental data for which the stressing voltage was 2.25□V and tunnel current 1□nA. (b) A schematic drawing of the real-time BEEM current plot with labels on the various stages.

Figure 6. Schematic drawings of the state of the interface at various stages of the terrace growth process. (a) During the latency period, the adatoms which are created diffuse away. (b) Eventually some adatoms coagulate to form a small terrace, but the terrace is not thermodynamically stable since the curvature is very large. The evaporation rate of atoms is high so the terrace grows slowly. The small terrace allows the BEEM current to increase somewhat. This is the situation as the BEEM current rises in the plots of Fig.□5.

Figure 7. (a) The latency time is plotted as a function of voltage. Different symbols correspond to measurements at different currents, i.e. +, *, and x correspond to 0.1, 1.0, and 3.0□nA tunnel current, respectively. The latency times have been scaled (using the

relation that the latency time is inversely proportional to the tunnel current) to their equivalent values at 1□A tunnel current. The solid line is from a model calculation described in the text. (b) The rate of rise of the BEEM current is shown as a function of bias voltage by plotting the time it takes for the BEEM current to get half way to its saturation value. The solid line is the model calculation. (c) A lower bound on the adatom production rate at 1□A calculated from the areal growth rate of the terraces is shown as a function of sample-tip voltage. The solid line is from the model calculation. The initial slope is ~5.92. Note the change in voltage dependence as the center of the threshold energy distribution is reached.

Figure 8. The increase in terrace area is shown as a function of hot electron dose is shown for several voltages. Note the initial increase is linear. (a) shows the raw data. (b)□shows the same data scaled to emphasize the similarity of the functional forms at different stressing biases.

Figure 9. When a hot electron inelastically scatters from a gold atom, it may break a bond causing the atom to become unstable in its present location. A schematic potential energy vs. position is shown indicating how an atom can be accelerated onto a surface by a potential energy gradient if the bond remains broken long enough.

Figure 10. A BEEM I-V spectra taken to a very high bias is shown. Note the dips in the BEEM current at higher voltages. These are attributed to electron-hole pair formation in the gold by inelastic scattering of the injected hot electrons. The scattering reduces the number of injected electrons which reach the interface so causes a reduction in the BEEM current near resonance.

Figure 11. Gray scale 1.4□V constant 1□A current STM (left) and corresponding BEEM (right) images illustrate various modifications of a type 1 sample. The images are 1800□Å square. (a) shows the STM topograph which exhibited some grain growth as a result of the intermixing modifications. (b) is the BEEM image which was uniformly gray before stressing with the STM current. The top, left and center intermixing modifications were created with 3.1□V and 3□A for 5.4 sec, 0.1□A for 5.4 sec, and 3□A for 2.7 sec, respectively. The creation of the lines near the bottom and right is described in the text.

Figure 12. Sketches of mechanisms which can result in the local decrease of the BEEM current from surrounding values. (a) A high density of defects such as vacancies within the bulk of the film can strongly scatter injected electrons leading to a decrease in the BEEM current. (b) An interfacial layer can also scatter electrons to reduce the BEEM current.

Figure 13. Plots of the BEEM current taken in real-time during modifications of the sample. The sample-tip bias was increased from the imaging value of 1.4□V linearly to the stressing value, at which it was held constant for a period of time, then decreased linearly back to the imaging value. The dotted lines indicate the times at which the bias reached and left the highest stressing value. The stressing voltages and tunnel current values for the plots are: (a) 2.1□V, 0.3□A, and (b) 1.9□V, 1□A. Although the various stages shown in Fig.□(b) are observed, periods of time when the BEEM current is strongly decreased from its expected value are found. We expect that vacancies produced in conjunction with the adatoms are within the path of and scattering the injected electrons

during these periods. These are blatent examples of a major source of noise in the real-time measurements -- the interface through which the BEEM electrons pass is being modified.

Figure 14. A sequence of gray scale 1.4□V constant current STM (top) and corresponding BEEM current (below) images show a region 1800□Å square of a type 2 sample (a-b) before, (c-d) just after, and (e-f) just under one half hour after the tip was held over the grain near the center of the image while the tunnel bias was increased to 3.5□V for 3□sec at a 1□nA tunnel current. (a,c,e) are the STM topographs with gray range 95□Å. The gold grains are up to 60□Å tall. (b,d,f) are the corresponding BEEM images shown with a 12□pA range. The enhanced features (~11-15□pA) appear whitish, background features (5-8□pA) gray, and degraded features (0□pA) black. Note that the changes in the BEEM images are correlated to the changes in the STM images. The enhanced region in (f) later disappeared.

Figure 15. Plots of the BEEM current taken in real-time during modifications of the sample help to determine the type of modification which is produced. (a,b) show the BEEM current as the interface is modified at a constant voltage. The dotted lines indicate when the voltage arrived at and departed that constant value. The starting and ending voltage values were the 1.4□V imaging bias. The current during stressing was 1□nA and the biases (a) 3.1□V and (b) 3.5□V. Note the different time axes. (c,d) show BEEM I-V spectra swept to high voltage to produce modifications. As above, the BEEM current is recorded for the entire time the bias voltage is away from the 1.4□V imaging value. Different symbols indicate different directions as the voltage is varied from 1.4□V to 0.4□V (circles), up to the maximum voltage (triangles), and back down to 1.4□V. The discontinuity in the circle data at 1.4□V represents the change in the BEEM current caused by the modification. Both processes degraded the local BEEM current. (c) produced a region with intermixing at the interface, later images resemble those in Fig.□1. (d) produced a large gold mound in addition to a BEEM current decrease.

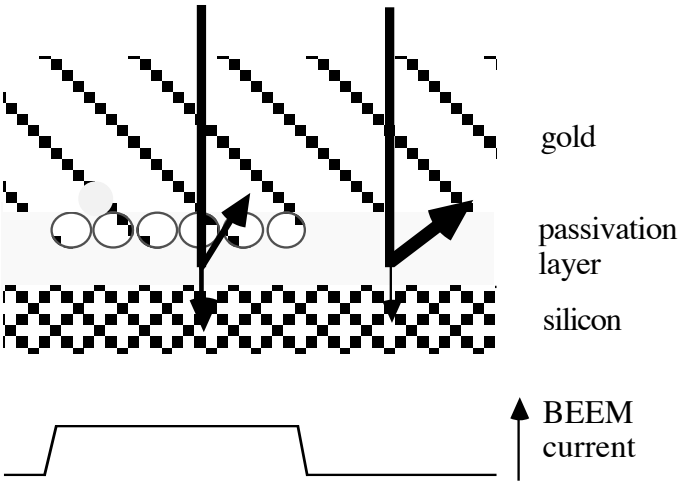

Figure 1.

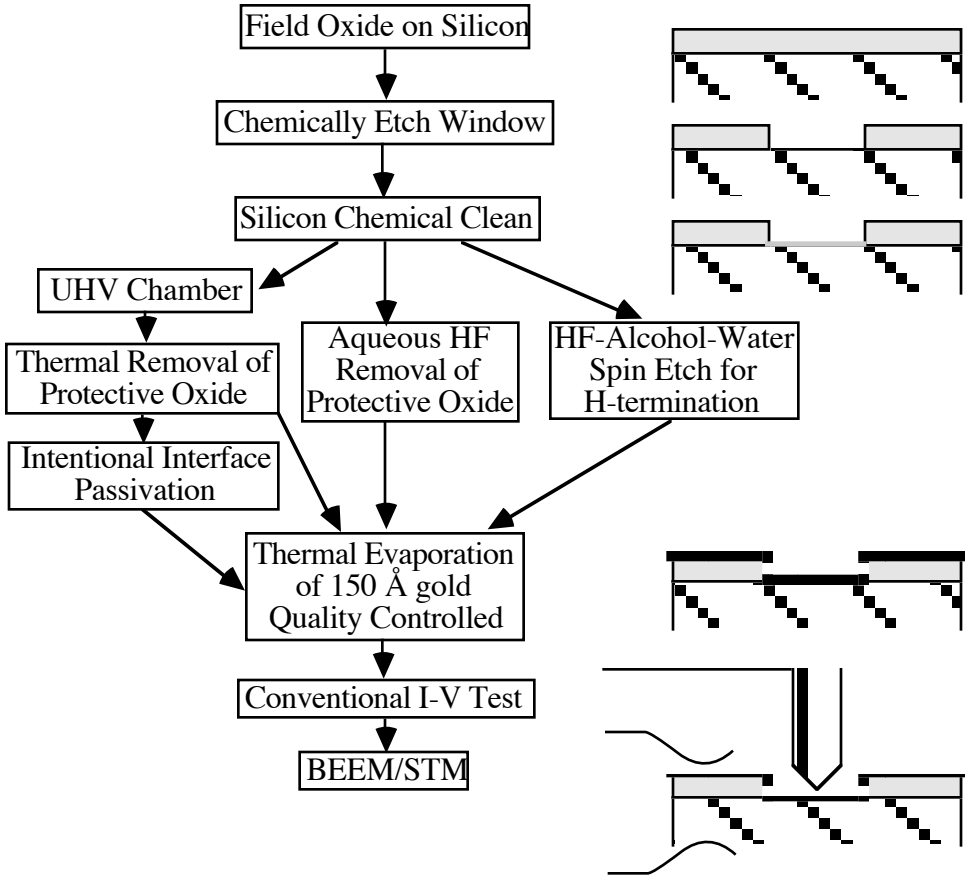
Field Oxide on Silicon
Chemically Etch Window
Silicon Chemical Clean
UHV Chamber
Thermal Removal of Protective Oxide
Intentional Interface Passivation
Aqueous HF Removal of Protective Oxide
HF-Alcohol-Water Spin Etch for H-termination
Thermal Evaporation of 150 Å gold Quality Controlled
Conventional I-V Test
BEEM/STM

Figure 3.

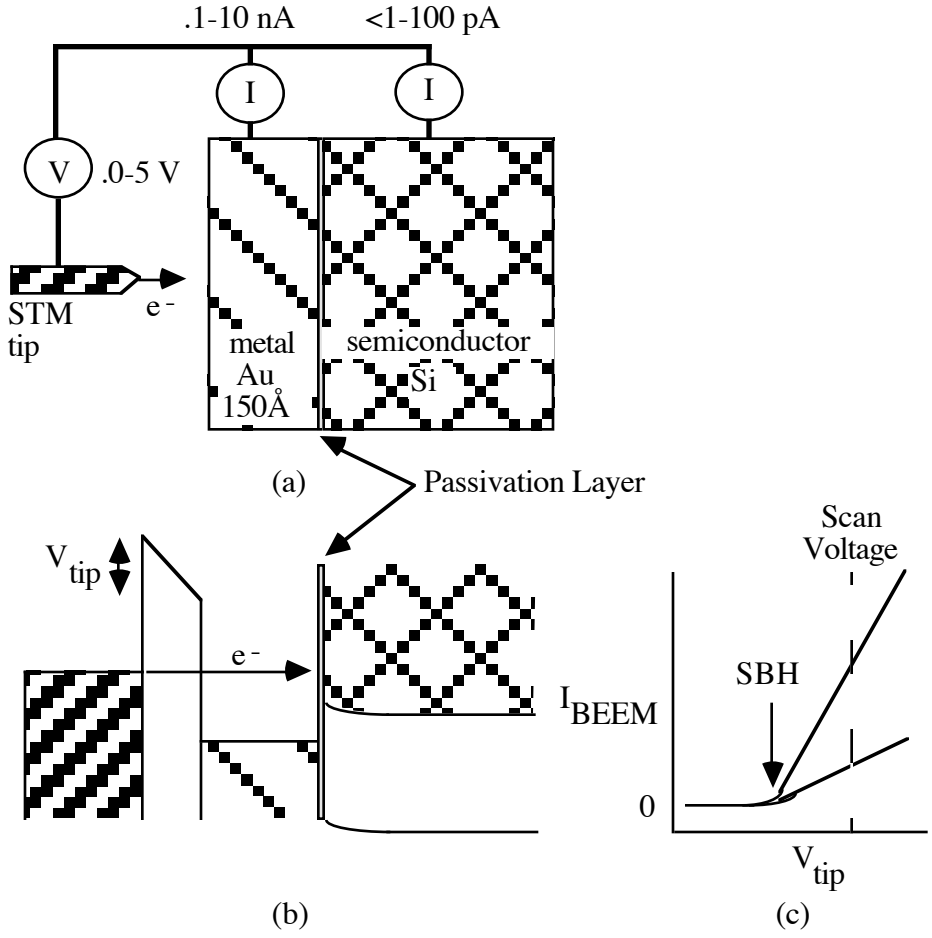
.1-10 nA
<1-100 pA
I
I
V
.0-5 V
STM
tip
e -
metal
Au
150Å
semiconductor
Si
(a)
Passivation Layer
V tip
e -
I BEEM
0
Scan
Voltage
SBH
V tip
(b)
(c)

Figure 4

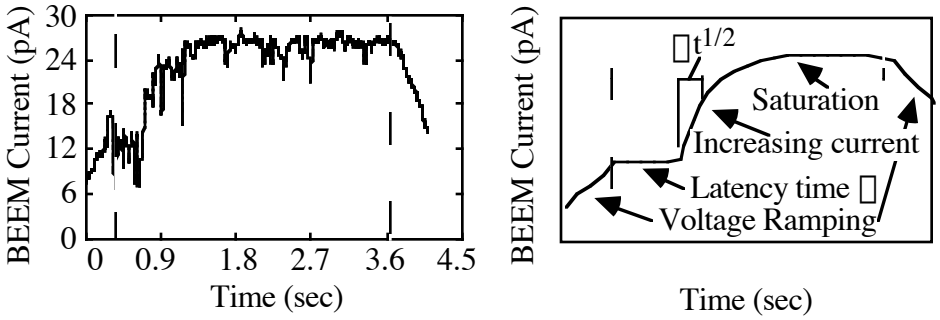
BEEM Current (pA)
30
24
18
12
6
0
0
0.9
1.8
2.7
3.6
4.5
Time (sec)
(a)
BEEM Current (pA)
t1/2
Saturation
Increasing current
Latency time
Voltage Ramping
Time (sec)
(b)

Figure 5

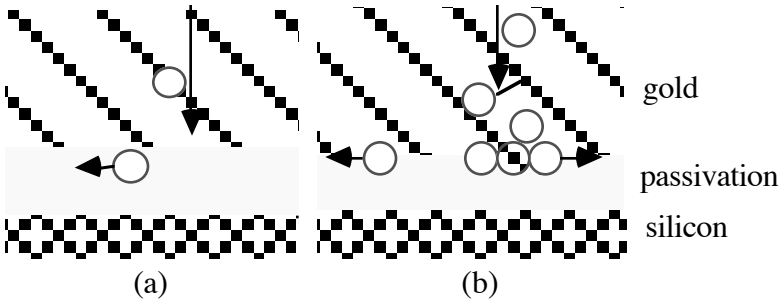

Figure 6.

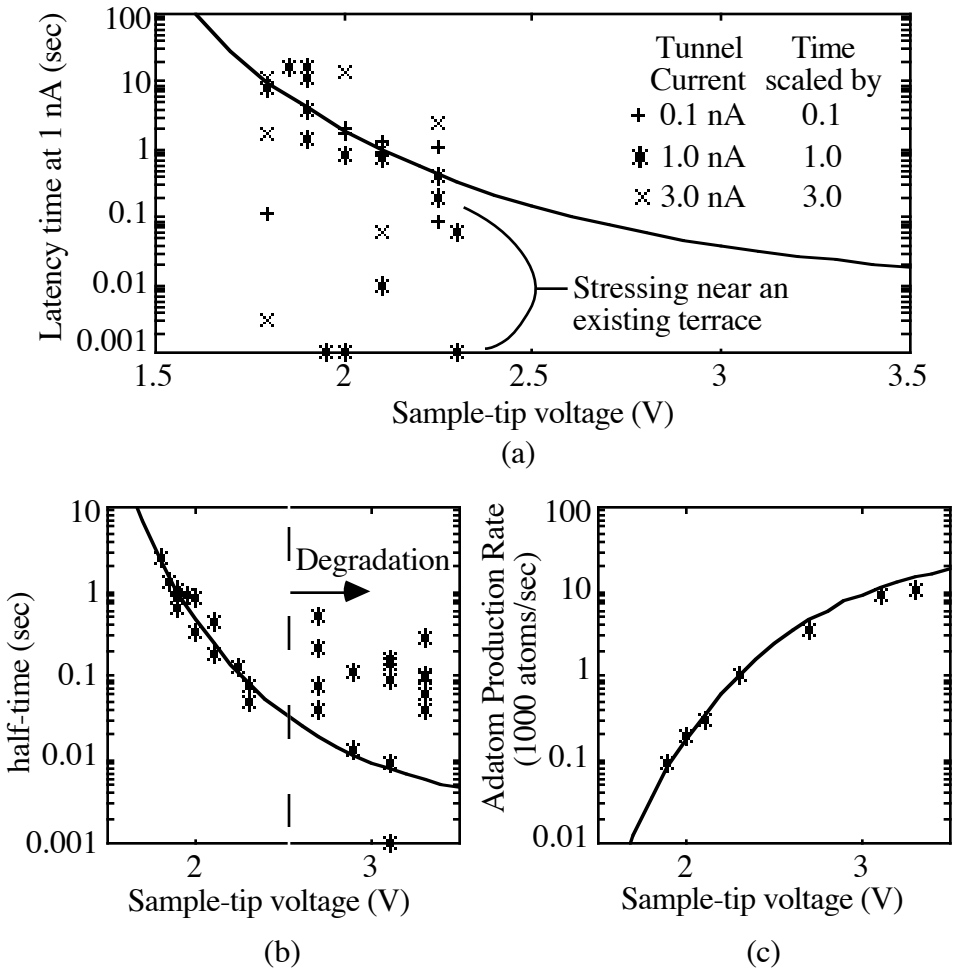
Latency time at 1 nA (sec)
100
10
1
0.1
0.01
0.001
1.5
2
2.5
3
3.5
Sample-tip voltage (V)
Tunnel Current
Time scaled by
0.1 nA 0.1
1.0 nA 1.0
3.0 nA 3.0
Stressing near an existing terrace
(a)
half-time (sec)
10
1
0.1
0.01
0.001
2
3
Sample-tip voltage (V)
Degradation
(b)
Adatom Production Rate (1000 atoms/sec)
100
10
1
0.1
0.01
2
3
Sample-tip voltage (V)
(c)

Figure 7.

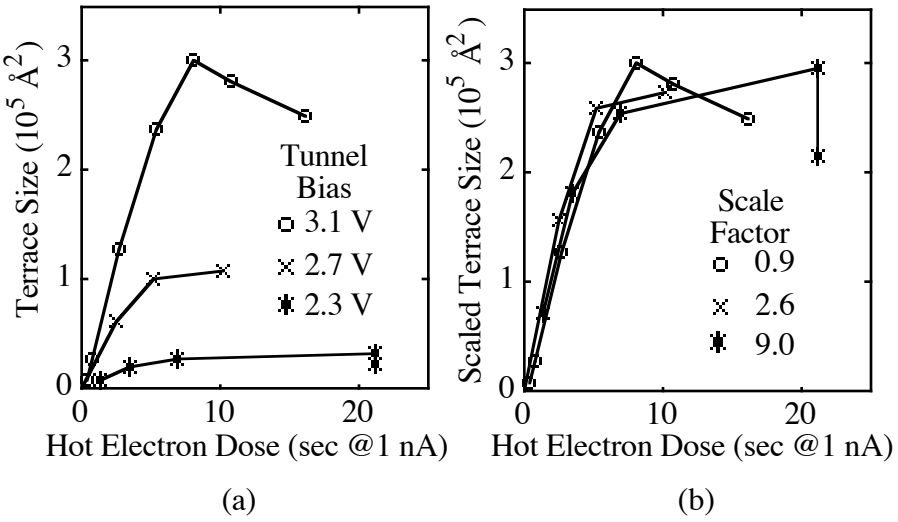
Terrace Size (10^5 Å^2)
Hot Electron Dose (sec @1 nA)
Tunnel Bias
3.1 V
2.7 V
2.3 V
(a)
Scaled Terrace Size (10^5 Å^2)
Hot Electron Dose (sec @1 nA)
Scale Factor
0.9
2.6
9.0
(b)

Figure 8.

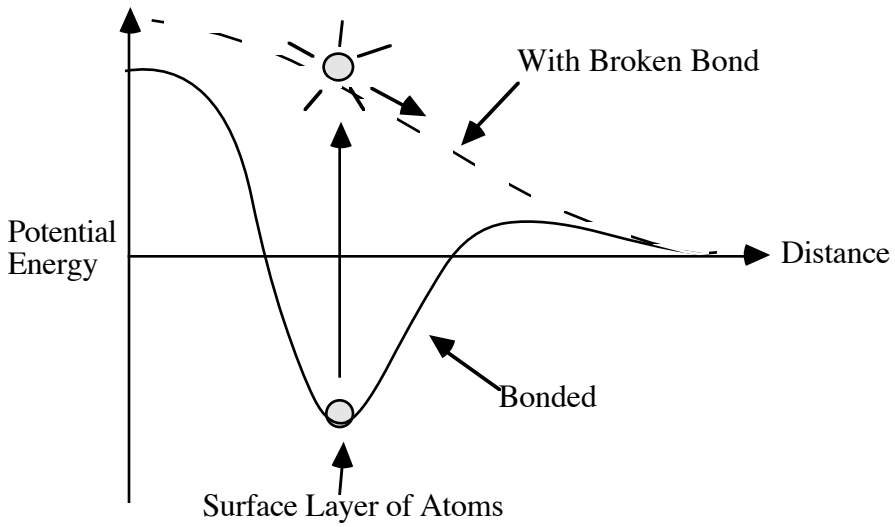
With Broken Bond
Potential
Energy
Distance
Bonded
Surface Layer of Atoms

Figure 9.

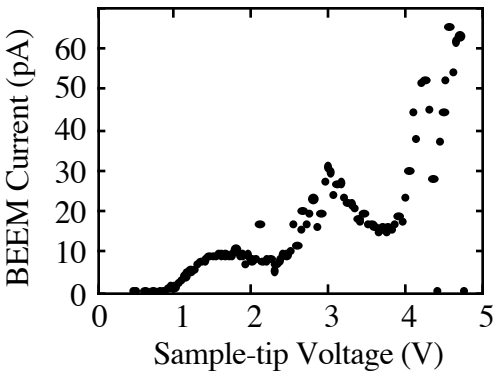

Figure 10.

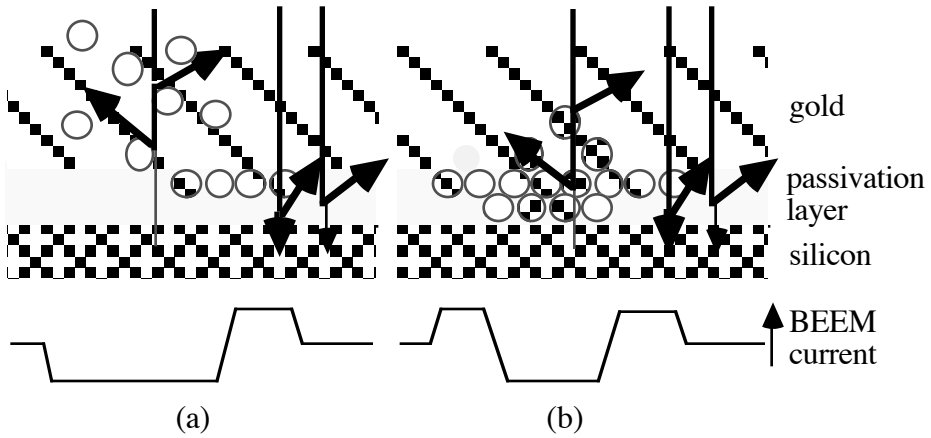

Figure 12.

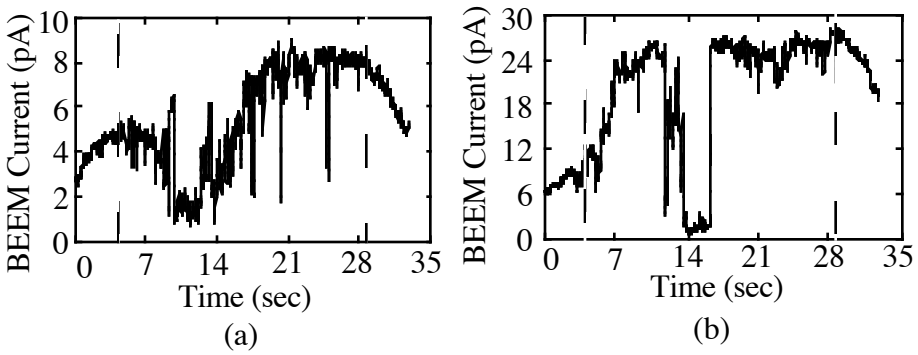
BEEM Current (pA)
10
8
6
4
2
0
0
7
14
21
28
35
Time (sec)
(a)
BEEM Current (pA)
30
24
18
12
6
0
0
7
14
21
28
35
Time (sec)
(b)

Figure 13.

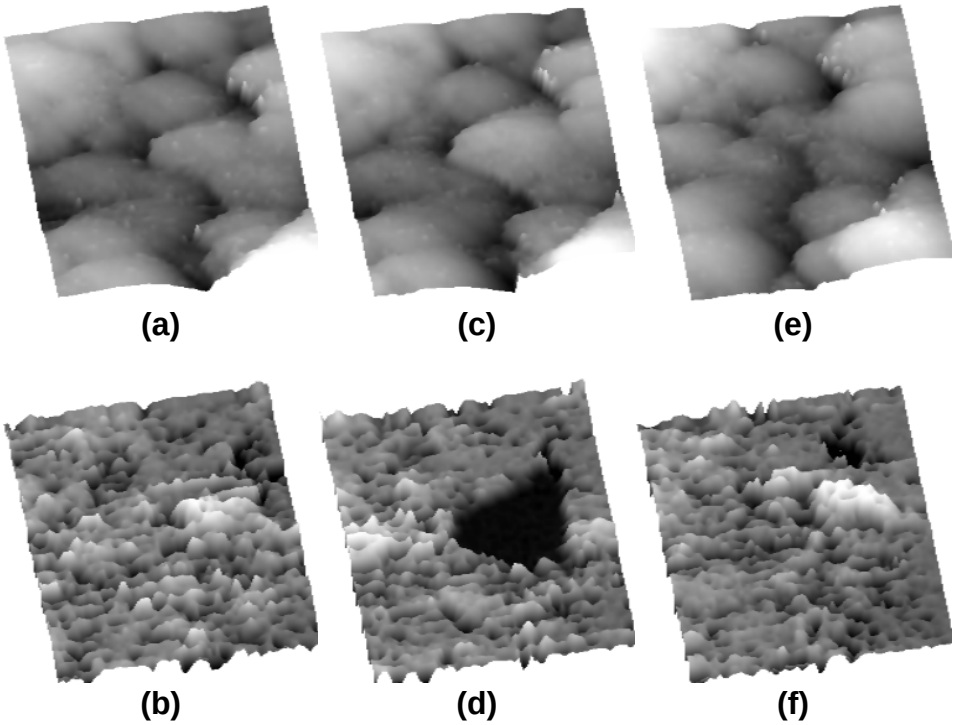
(a)
(c)
(e)
(b)
(d)
(f)

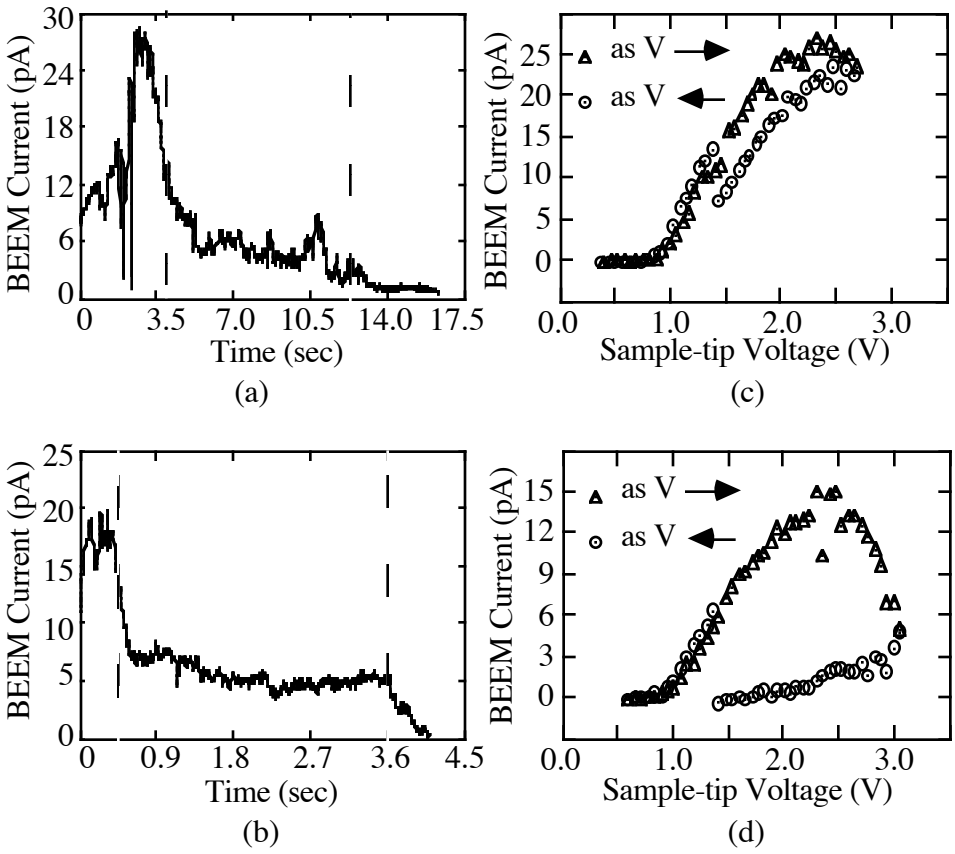
BEEM Current (pA)
Time (sec)
(a)
BEEM Current (pA)
as V
as V
Sample-tip Voltage (V)
(c)
BEEM Current (pA)
Time (sec)
(b)
BEEM Current (pA)
as V
as V
Sample-tip Voltage (V)
(d)

Figure 15